ADVANCED MATERIALS
www.advmat.de

Intrinsic Wettability in Pristine Graphene

Jincan Zhang, Kaicheng Jia, Yongfeng Huang, Xiaoting Liu, Qiuhao Xu, Wendong Wang, Rui Zhang, Bingyao Liu, Liming Zheng, Heng Chen, Peng Gao, Sheng Meng, Li Lin,* Hailin Peng,* and Zhongfan Liu**

The wettability of graphene remains controversial owing to its high sensitivity to the surroundings, which is reflected by the wide range of reported water contact angle (WCA). Specifically, the surface contamination and underlying substrate would strongly alter the intrinsic wettability of graphene. Here, the intrinsic wettability of graphene is investigated by measuring WCA on suspended, superclean graphene membrane using environmental scanning electron microscope. An extremely low WCA with an average value ≈30° is observed, confirming the hydrophilic nature of pristine graphene. This high hydrophilicity originates from the charge transfer between graphene and water molecules through H–π interaction. The work provides a deep understanding of the water–graphene interaction and opens up a new way for measuring the surface properties of 2D materials.

1. Introduction

The wettability of graphene is vital for enormous emerging applications, such as ion sieving,[1] water permeation,[2] water conformal coating,[3] and energy storage.[4] At 2D regime, surface properties of 2D materials, including wettability, roughness, and adhesion,[5] become severely sensitive to the surroundings, as a result of which the intrinsic wettability of graphene remains elusive.[6,7] Two surrounding factors, surface contamination[8,9] and substrate interference,[10–12] would strongly alter the wetting ability of graphene, which, however, have not been avoided at the same time. Therefore, a controversy on the wettability of graphene still remains,[6,7,13] and the intrinsic wettability of graphene has not been accurately determined, which is clearly reflected by the wide range of reported water contact angles (WCAs).[7,10,14,15] Specifically, graphene was initially believed to be hydrophobic with a WCA over 80° and possess the wetting transparent nature, in which the wettability of graphene would be dramatically altered by substrates via charge transfer and surface fluctuation.[9,11] However, the removal of surface contamination enabled the observation of a reduced water contact angle; therefore, it is believed that the surface contamination mainly modifies the wettability of graphene.[8,9] To clear this controversy, it is crucial to explore the basic interaction between water and graphene, and probe the intrinsic wettability of graphene by validating the contributions from both substrates and surface contamination.

J. C. Zhang, K. C. Jia, X. T. Liu, L. M. Zheng, H. Chen, H. L. Peng, Z. F. Liu
Center for Nanochemistry
Beijing Science and Engineering Center for Nanocarbons
Beijing National Laboratory for Molecular Sciences
College of Chemistry and Molecular Engineering
Peking University
Beijing 100871, P. R. China
E-mail: hlpeng@pku.edu.cn; zfliu@pku.edu.cn

J. C. Zhang, K. C. Jia, X. T. Liu, B. Y. Liu, L. M. Zheng, H. Chen, H. L. Peng, Z. F. Liu
Beijing Graphene Institute
Beijing 100095, P. R. China

J. C. Zhang
Department of Engineering
University of Cambridge
Cambridge CB3 0FA, UK

J. C. Zhang, X. T. Liu, B. Y. Liu
Academy for Advanced Interdisciplinary Studies
Peking University
Beijing 100871, P. R. China

Y. F. Huang, S. Meng
Songshan Lake Materials Laboratory
Dongguan, Guangdong 523808, P. R. China
E-mail: smeng@iphy.ac.cn

The ORCID identification number(s) for the author(s) of this article can be found under https://doi.org/10.1002/adma.202103620.

DOI: 10.1002/adma.202103620

Y. F. Huang, Q. H. Xu, S. Meng
Beijing National Laboratory for Condensed Matter Physics and Institute of Physics
Chinese Academy of Sciences
Beijing 100190, P. R. China

Q. H. Xu, S. Meng
School of Physical Sciences
University of Chinese Academy of Sciences
Beijing 100049, P. R. China

W. D. Wang, R. Zhang
Department of Physics and Astronomy
University of Manchester
Manchester M13 9PL, UK

B. Y. Liu, P. Gao
Electron Microscopy Laboratory and International Center for Quantum Materials
School of Physics
Peking University
Beijing 100871, P. R. China

P. Gao
Collaborative Innovation Center of Quantum Matter
Beijing 100871, P. R. China

L. Lin
Materials Science and Engineering
National University of Singapore
Singapore 119077, Singapore
E-mail: linli-cnc@pku.edu.cn

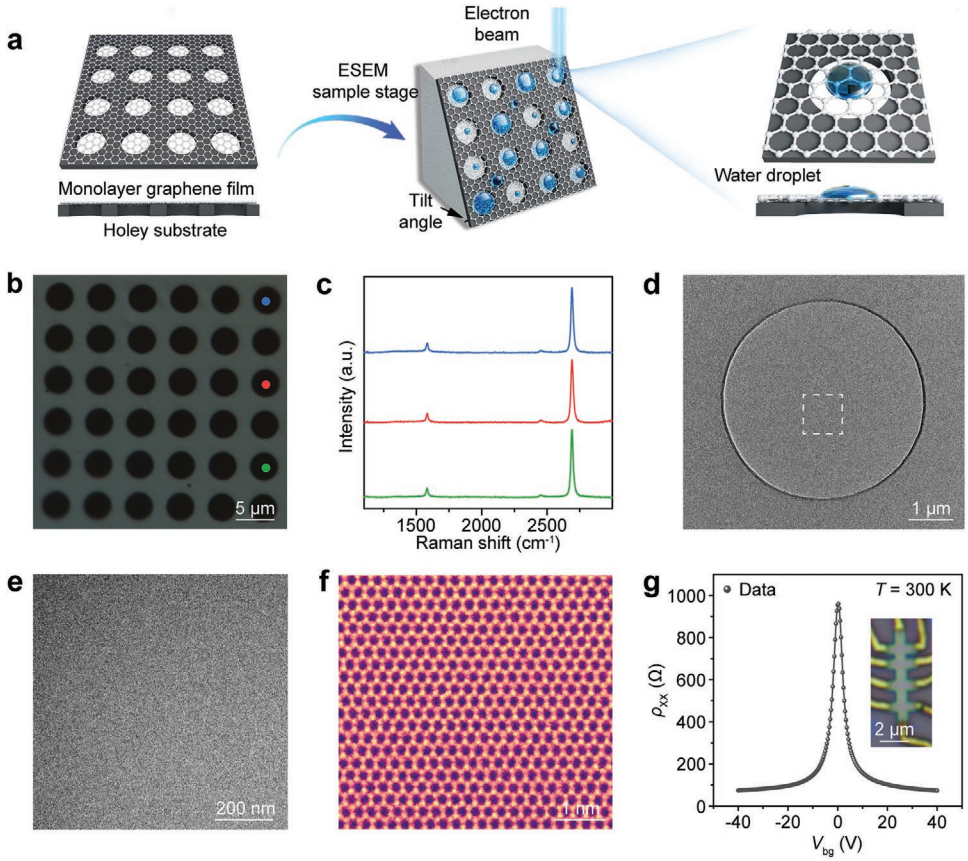

Figure 1. Preparation of large-area high-quality superclean suspended graphene membrane for ESEM measurement. a) Illustration of the ESEM imaging of water droplets on suspended graphene. b) Optical microscopy (OM) image of the suspended graphene sample transferred onto holey substrate. c) Typical Raman spectra of the suspended graphene measured at the marked positions in (b). d) Low-magnification TEM images of the transferred suspended graphene membrane. e) TEM image of the square region marked in (d). f) Representative atomically resolved scanning TEM (STEM) image of the suspended graphene. g) Resistivity as a function of the gate voltage. Inset: OM image of the Hall-bar device.

However, current challenges of preparing contamination-free and suspended graphene membrane in large scale severely hamper the precise measurement of the intrinsic wettability of graphene.[16,17] Chemical vapor deposition (CVD) method delivers a chance to grow large-area, high-quality graphene film with comparable quality to its mechanical exfoliated counterpart,[16,18] and to fabricate suspended graphene membrane free of surface contamination.[19] However, current static WCA measurement methods with millimeter-sized detecting region,[14] require a larger free-standing region of graphene membrane beyond the reach of existing methods for fabricating suspended CVD graphene.[20] Therefore, the accurate measurement of graphene WCAs remains unachievable.

Herein, intrinsic wettability of graphene is clearly determined via the measurement of WCAs on suspended, superclean graphene membrane, with the assistance of environmental scanning electron microscope (ESEM) (**Figure 1**a). An extremely low WCA with an average value ≈30° is observed after excluding the interference by substrates and contamination, which clearly confirms the hydrophilic nature of pristine graphene. Such hydrophilic property is revealed to be caused by charge transfer between graphene and water through H–π interaction. This work not only provides a deep understanding of the interaction between water and graphene, but also delivers a strategy for measuring the surface properties of graphene and other 2D materials.

2. Results and Discussion

To remove surface contamination, the formation of amorphous carbon on the surface of CVD graphene is successfully inhibited with the assistance of Cu foam during the synthesis.[18] Subsequently, polymer-free transfer method is employed to transfer graphene onto ultraflat Au/carbon-film grid with arrays of circular holes (diameter ≈ 4 μm), so that suspended graphene membrane is fabricated for WCA measurement in absence of contamination (Figure 1b; Figure S1a,b, Supporting Information).[19] Note that, Au film is coated atop the holey carbon film before graphene transfer in order to improve the conductivity of the sample and further enhance the subsequent resolution of ESEM characterization. Raman spectroscopy is conducted to confirm the high crystallinity of graphene. The absence of D peak and the high intensity ratio of 2D to G bands (I_{2D}/I_G) suggest the high quality of the suspended graphene membrane.[20] (Figure 1c; Figures S2 and S3, Supporting information). Specifically, owing to its low defect density and low doping level without the interference from the substrates, the high

I_{2D}/I_G in the Raman spectra of the suspended graphene, with an average of 7.2, further confirms high quality of the pristine graphene used in our wettability measurement.[21,22] Scanning electron microscopy (SEM) observation confirms the high intactness of suspended graphene over a large area (Figure S1c, Supporting Information). Low-magnification transmission electron microscope (TEM) images indicate the high cleanness of the suspended membrane, with the uniform and light contrast in the whole hole (Figure 1d,e; Figure S1d, Supporting Information). Meanwhile, the individual carbon atoms in graphene are distinguishable in high-resolution TEM (HRTEM) images while no amorphous structure is observed (Figure 1f; Figure S1e, Supporting Information). Besides, the high cleanness of as-prepared graphene membrane is also confirmed using atomic force microscope (AFM) (Figure S1f, Supporting Information). The high carrier mobility (μ_h = 6.6 × 10^4 cm^2 V^{-1} s^{-1} and μ_e = 6.4 × 10^4 cm^2 V^{-1} s^{-1} at room temperature) (Figure 1g; Figure S4, Supporting Information), which is comparable to those of mechanically exfoliated graphene, further confirms the high surface cleanness and low defect density of the graphene film.

By slowly increasing the water pressure from vacuum state in ESEM chamber, micrometer-sized water droplets, for which the impact of gravity can be ignored,[23] are formed on the surface of suspended graphene membrane. The stage is cooled to a low temperature (−2 to 3 °C) to enable the formation of clearly visible and stable water droplets with legible outlines. We measure the contact angle of water droplets formed on suspended graphene to exclude the interference from the substrates (**Figure 2**a; Figure S5, Supporting Information), since the substrate is found to have noticeable influences on the measurement of WCAs of graphene (Figure 2b; Figure S6, Supporting information), which has been widely reported before.[10,14] We can acquire ESEM images with improved contrast and resolution after tuning tilt angles of the stage (Figure 2c–f; Figure S7, Supporting information), and observe the uniform distribution of water droplets on suspended graphene surface (Figure 2f). Based on the statistic of over 200 water droplets, the obtained WCAs on suspended graphene locate around 30° (Figure S8, Supporting Information). Meanwhile, the measured WCAs exhibit almost no changes with experimental conditions including the tilt angle of sample, the size of water droplets, and the temperature of cooling stage (Figure 2g–i), so that the obtained WCAs in our method should reflect the intrinsic wettability of graphene materials (Figure S9, Supporting information). We therefore conclude that pristine graphene has high hydrophilicity, and the WCA of pristine graphene in this work is lower than previously reported values, because the influences

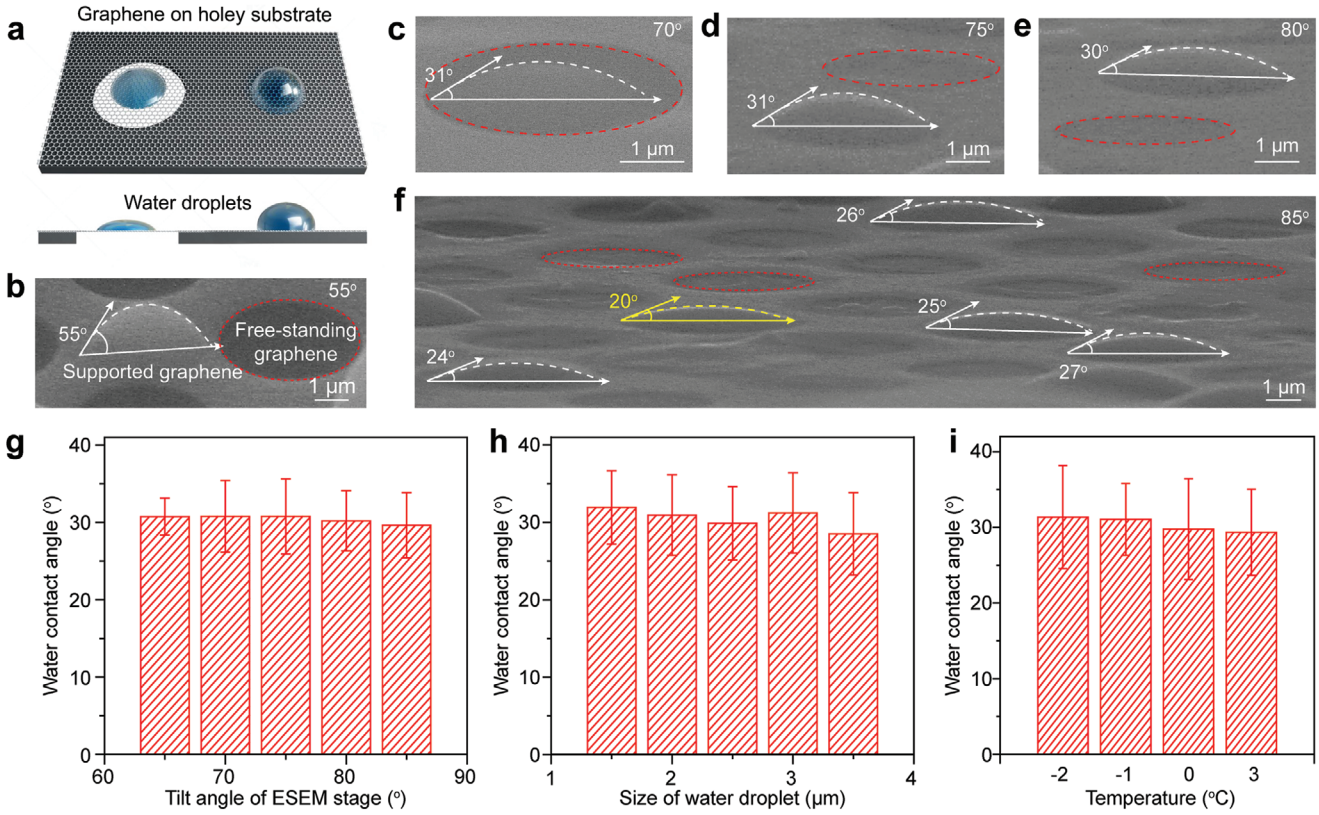

Figure 2. Intrinsic wettability of graphene measured by ESEM. a) Schematic of intrinsic wettability of pristine graphene and the impact of the substrate. b) ESEM image of water droplet on the graphene supported by the Au/carbon film substrate. c–f) Typical ESEM images of water droplets on the surface of suspended graphene with the tilt angles of sample stage with respect to the electron beam of c) 70°, d) 75°, e) 80°, and f) 85°, respectively. The red circles highlight the region of the suspended graphene, and the white arc lines denote the outlines of water droplets. g) Statistical results of the WCA values measured at different tilt angles. h) Statistical WCA values of water droplets with different sizes. i) Statistical results of the WCA values measured at different temperature.

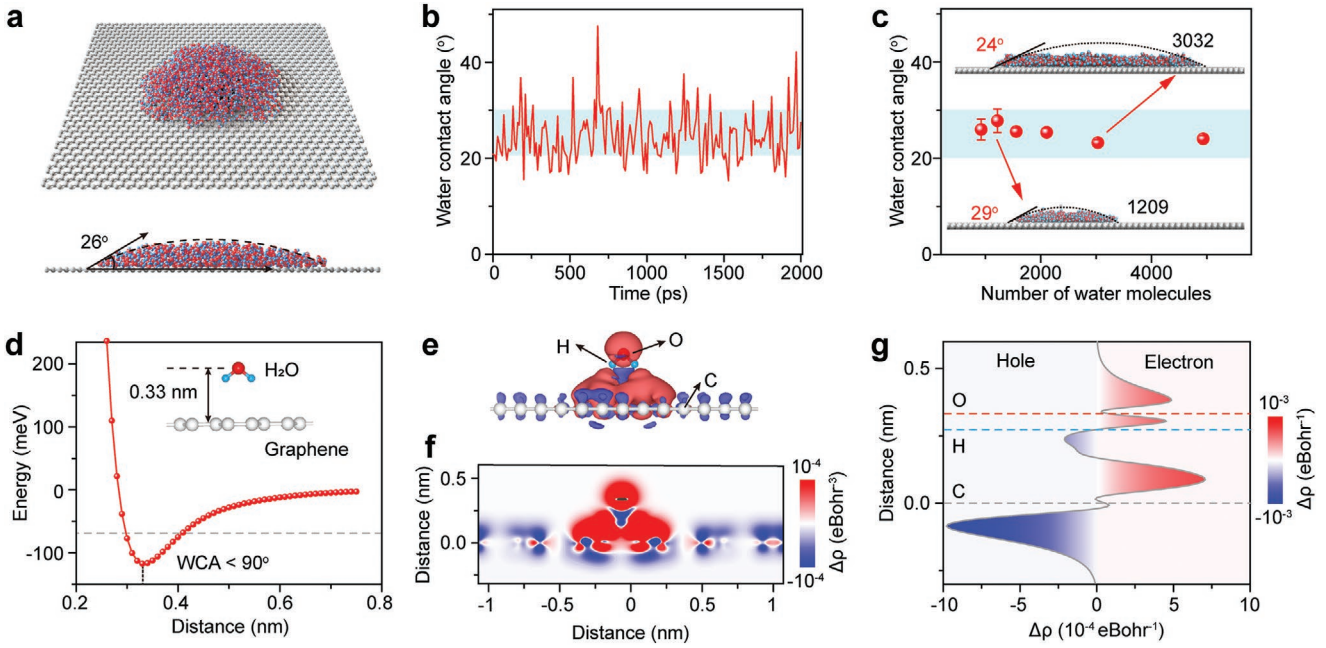

Figure 3. Theoretical analysis of the intrinsic wettability of graphene. a) MD simulation result showing the spatial distribution of water molecules on pristine graphene. b) Temporal evolution of the WCAs of free-standing graphene after the relaxation of water molecules reaching the stable state. c) MD simulation results of the WCAs of graphene with different number of water molecules. Inset: Typical side views of the water droplets composed of 3032 (top) and 1209 (bottom) molecules. d) Adsorption energy as the function of distance for a water molecule adsorbed on the surface of free-standing graphene. Inset: Side view of one water molecule adsorbed on graphene surface with two hydrogen atoms pointing to the graphene plane. e) 3D and f) 2D results of accurate first-principles simulations of the charge transfer between water molecule and graphene. Red and blue clouds represent the accumulation and depletion of electrons, respectively. g) Planar-averaged electron density difference as a function of the distance to the graphene plane.

from both substrates and surface contamination are avoided (Table S1, Supporting Information).

Molecular dynamics (MD) and first-principles simulations are performed to investigate the water–graphene interaction to understand the wettability of graphene. In the MD simulations, relaxation of thousands of water molecules on graphene surface (4 ns to reach the stable state) is conducted (**Figure 3**a). By fitting the hemispherical-shaped water droplet using Young-Laplace modulus, we obtain the simulated WCAs, which have an average value of ≈26° (Figure 3b; Figure S10a, Supporting Information), consistent with experimentally observed wettability of graphene. Meanwhile, no obvious change of WCA is observed by changing the simulation temperature (Figure S10b, Supporting Information) or increasing the number of water molecules from 927 to 4934 (Figure 3c), indicating that the size of water droplets and temperature would not affect significantly the wetting behaviours of graphene.

Accurate first-principles simulations are further conducted to probe the water–graphene interaction. In this regard, both "one-leg" and "two-leg" configurations are constructed to represent the structures of water molecules with one or two H atoms approaching the graphene plane, respectively. The adsorption energy of the water molecule on graphene is calculated accordingly, which depends on the distance between the oxygen atom in water molecule and the graphene plane (Figure 3d). The adsorption energy of water molecule on graphene is no larger than –117.5 meV, consistent with the observed high hydrophilicity of graphene.[24]

Based on the maximum adsorption energy of water molecule on graphene, we obtain a proper distance between graphene and water molecule, and then analyze the corresponding charge distribution in the water–graphene system (Figures S11 and S12, Supporting Information). In the "two-leg" configuration, the stable distance between water molecule and graphene is 0.33 nm (Figure 3d). Then, the charge transfer from graphene to water molecule is calculated. The electron transfers from the π bands of graphene towards H atoms in water molecule (Figure 3e), resulting in the formation of H–π interaction, which accounts for the intrinsic hydrophilicity of graphene. In addition, the water molecule would impact the charge distribution of graphene in larger than 2 nm region, as revealed by the profile map of the charge distribution (Figure 3f). The total amount of charges transferred from graphene to water molecule along the z-direction is 0.0221 electron, as presented in the planar-averaged electron density as a function of water height (Figure 3g). Similar H–π interaction between graphene and water molecule is also observed in the one-leg configuration (Figure S12, Supporting Information).

Wettability of graphene, as one of key surface properties, is very sensitive to underlying substrates (Figure 2a,b) and surface contamination (**Figure 4**a). For example, if using Au film as the substrate to support graphene, WCA of graphene increases from ≈30° (suspended) to ≈55° (supported) (Figure 2b). The observed WCAs are lower than that of pure Au film (≈73°, Figure S13, Supporting Information); therefore, this observation confirms the partial-wetting transparency of graphene, consistent with the previously reported results.[7] As reported recently, high-temperature CVD synthesis process is mainly responsible for the formation of surface contamination, such as amorphous

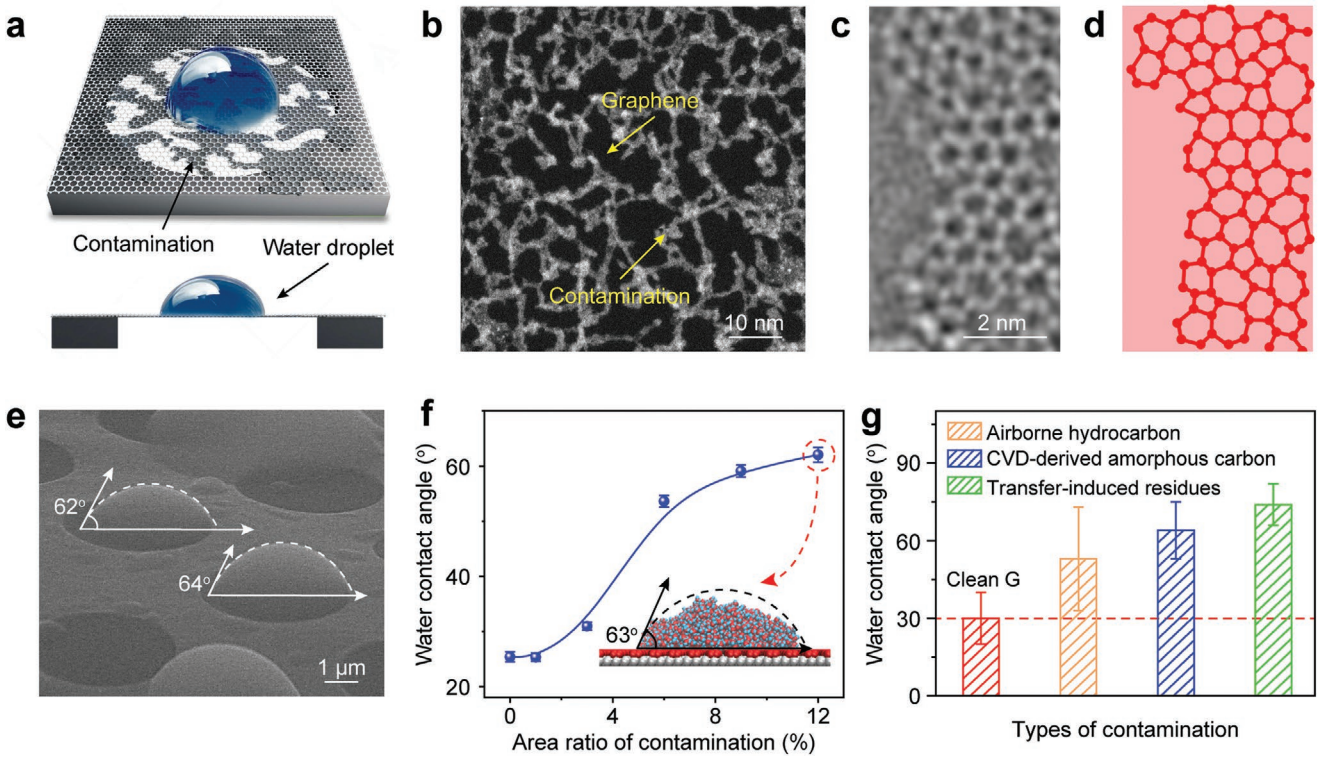

Figure 4. Impact of surface contamination on the wettability of graphene. a) Schematic illustration of the wettability of contaminated graphene. b) Low-magnification STEM image of graphene contaminated by amorphous carbon. c) Structure of amorphous carbon contamination on graphene based on fast Fourier transform mask filter to remove graphene structure beneath and d) the corresponding atomistic model of the amorphous carbon contamination. e) Representative ESEM image of water droplets on suspended contaminated graphene surface. f) WCA values of graphene as a function of the coverage of contamination on graphene surface. Inset: Typical MD simulation image showing the distribution of water molecules on graphene surface contaminated by pentagon. g) Statistics of WCAs of graphene contaminated by airborne hydrocarbon (orange), CVD-derived amorphous carbon (blue), transfer-induced residues (green), and clean graphene (red).

carbon, on graphene surface.[18,24] As observed in the TEM image, the universal distribution of amorphous carbon leaves the lateral size of continuous clean regions smaller than 100 nm (Figure 4b). The contamination on graphene surface mainly consists of carbon octagon, heptagon, pentagon, and distorted hexagon (Figure 4c,d). In the ESEM images of water droplets on suspended graphene contaminated by amorphous carbon, the measured WCAs are over 60°, higher than that of clean graphene, verifying the influence of contamination on the wettability of graphene (Figure 4e; Figure S14, Supporting information). Based on the observed structure of amorphous carbon, simplified models are built to represent the contaminated graphene and to investigate the influence of surface contamination upon the wettability of graphene (Figure S15, Supporting Information). First, graphene with the presence of carbon pentagon as contamination on the surface exhibits an increased WCA in the MD simulations, consistent with the experimental results in Figure 4e. Water molecules exist on the top of amorphous carbon instead of occupying the space between amorphous carbon (Figure S16, Supporting Information). Therefore, the water molecules are prone to form a Cassie–Baxter wetting state on the contaminated graphene: the surface contamination, acting as the atomic decoration of graphene surface,[26] would weaken the H–π interaction between graphene and water molecules, and result in a larger WCA.[12,27] The correspondence between contamination and graphene wettability is validated by the increased WCAs of graphene with a high coverage of surface contamination in the MD simulations (Figure 4f). In addition, we simulate the wettability of graphene covered by Stone-Wales defect structures as contamination, and observe a similar increased WCA as well (Figure S15b, Supporting Information). Moreover, first-principles simulations were conducted using stone-Wales defect structure as the simplified structure of amorphous carbon contamination, which further indicates the blocked H–π interaction between water molecule and graphene after the presence of amorphous carbon contamination on graphene surface (Figure S17, Supporting Information).

Besides the amorphous carbon formed during the high-temperature CVD growth process, we found that the presence of airborne hydrocarbon (Figures S18 Figure S19, Supporting Information) and transfer-induced polymer residues would also increase the WCAs of graphene (Figure 4g; Figure S11, Supporting Information), suggesting that the existence of surface contamination is one of the main causes for the commonly observed hydrophobic behaviours of graphene film.

3. Conclusion

In conclusion, using ESEM, we confirm the high hydrophilic nature of pristine graphene with an extremely low WCA of

≈30°, since the interference from both substrate and surface contamination are excluded. The high hydrophilic property of graphene is revealed to originate from charge transfer between graphene and water molecules through H–π interaction. Our method for probing the surface properties can be extended to other 2D materials. More importantly, the revelation of the intrinsic wettability of graphene ends the previous controversy, and is very important to accelerate the research in the areas of both fundamental science and new applications regarding the surface properties of graphene and other 2D materials.

4. Experimental Section

Graphene Growth and Transfer: Monolayer graphene films are synthesized in a low-pressure hot-wall CVD system, referring to the previously reported work.[18] 25 µm-thick copper foil (Alfa Aesar 46 365#) was utilized as the growth substrate after electrochemical polishing. In detail, the annealing and growth temperature was set to 1020 °C. First, Cu foil was annealed in reductive atmosphere (H_2, 100 sccm) for 30 min to flatten its surface and eliminate organic contamination. Subsequently, H_2 (100 sccm) and CH_4 (1 sccm) are introduced into the chamber to initiate the growth of graphene film for 10–60 min. After growth, the CVD system was cooled down with the same gas supply. In particular, Cu foam was utilized to supply extra Cu vapor during the high-temperature growth of graphene, in order to suppress the formation of amorphous carbon contamination and improve the cleanness of CVD-derived graphene.

The as-grown graphene film was transferred onto SiO_2/Si substrate with the assistance of polymethyl methacrylate (PMMA). First, PMMA was first spun coated onto graphene/Cu sample at 2000 rpm and then baked at 170 °C for 5 min. $Na_2S_2O_8$ solution (1 mol L^{-1}) was utilized for the etching of Cu substrate to acquire free-standing PMMA/graphene film. After being rinsed with deionized water, the PMMA/graphene film was subsequently transferred onto SiO_2/Si substrate. Finally, hot acetone was used to remove PMMA from the surface of graphene.

To avoid the disturbance from transfer-induced polymer residues, a polymer-free clean transfer method[19] was employed to fabricate superclean suspended graphene membrane for WCA measurement. Commercial TEM grid (diameter ≈ 3 mm) with arrays of holes (diameter ≈ 4 µm, distance ≈ 2 µm) was selected as the target substrate for the transfer of graphene film, which was beneficial for the preparation of suspended graphene with regular shape and high intactness. The TEM grid was coated with Au film (50 nm) by thermal evaporation at a deposition rate of 0.01 nm s^{-1} before transferring graphene.

After CVD growth of graphene, the as-synthesized graphene samples are put inside the clean glass containers, which are surrounded by dry ice in a heat preservation box and then taken to the ESEM lab. This was because that storing in low temperature could effectively avoid the adsorption of airborne contamination on graphene surface.[28] The polymer-free transfer of graphene was then conducted in the ESEM lab to guarantee that the ESEM characterizations can be conducted immediately after the preparation of the suspended graphene. To prepare the suspended graphene membrane, the Au-coated TEM grid was put atop the flat graphene/Cu sample (≈2.5 × 2.5 mm^2) supported by a clean glass plate, which has been thoroughly cleaned via ultrasonic treatment in acetone, water, and isopropyl alcohol (IPA) successively. After that, a drop of IPA (≈2 µL) was dropped to adhere the holey substrate to the graphene film tightly, followed by Cu etching in $Na_2S_2O_8$ solution (1 mol L^{-1}). The suspended graphene was then cleaned in large amount of distilled water by immersing the sample inside water for 10 min. After that the sample was washed by IPA for 3 min, whose low surface tension and high evaporation rate are beneficial to avoid breakage of the suspended graphene and accelerate the sample drying under nitrogen flow.

Graphene Characterization: The morphology and structure of as-received graphene are characterized using optical microscopy (Olympus BX51), SEM (FEI Quattro S, acceleration voltage 1–30 kV), AFM (Bruker dimension icon using the ScanAsyst mode), TEM (FEI Tecnai F30 and probe-corrected Nion electron microscope at an acceleration voltage of 300 and 60 kV, respectively) and Raman spectroscopy (Horiba, LabRAM HR-800, 532 nm laser wavelength, ×100 objective). The morphology and distribution of water droplets are characterized using Quattro ESEM (Thermo Fisher, acceleration voltage 5–30 kV) equipped with a cooling stage and water vapor supplier.

For the transport property measurement, the graphene film was encapsulated by relatively thick (≈40 nm) crystal of hexagonal boron nitride (hBN) to exclude the influence of substrate scattering. Besides, dry-peel technique with polydimethylsiloxane/poly (propylene carbonate) stack was utilized for the transfer of graphene with decreased transfer-related doping.[29,30] After this, the devices are fabricated using electron beam lithography and standard etching procedures for 1D contact electrodes (3 nm Cr and 80 nm Au), and Hall-bar shaping. The electrical properties of the fabricated devices are characterized using the conventional lock-in technique. An AC current I_{ds} with a root mean square amplitude of 1 µA at 23.33 Hz was applied between the source and drain terminals. Meanwhile, the four-point longitude voltage drop V_{xx} and transverse voltage drop V_{xy} are measured with lock-in amplifiers. The charge density tuning in the graphene channel was achieved by applying different back gate voltage V_{bg} to the SiO_2/Si substrate. To eliminate the negative effect of oxygen and water in air on the device performance, the device was tested in argon inertial environment (glovebox at the temperature of 300 K). Then, the longitude resistivity ρ_{xx} could be calculated from $\rho_{xx} = R_{xx} \times W/L$, where W is the width of the conducting channel, L is the length of the channel between the probed contacts, and R_{xx} is the longitude resistance, which can be calculated from $R_{xx} = V_{xx}/I_{ds}$. Thus, the result of longitude conductivity σ_{xx} can be obtained from ρ_{xx} via $\sigma_{xx} = 1/\rho_{xx}$. The Hall carrier density n is determined by $n = B/(eR_{xy})$, where e is the elementary charge and R_{xy} is the Hall resistance, which could be calculated from $R_{xy} = V_{xy}/I_{ds}$ at the corresponding perpendicular magnetic field B. Based on the Drude model, mobility $\mu = \sigma_{xx}/(ne)$ can be estimated from the slop of linear regions of σ_{xx} versus n plots.

MD and First-Principles Simulations: The graphene in the MD simulations was composed of 15 228 carbon atoms. Periodic boundary in three dimensions with the size of 19.921 nm × 20.022 nm × 20 nm was employed. The initial structure of the water droplet for MD simulation was a cubic water droplet with the size of 4 nm × 4 nm × 4 nm, containing 2109 water molecules above graphene with the distance of 0.5 nm. SPC water model is applied and carbon atoms of graphene are frozen during MD simulations.[31] The isothermal-isochoric ensemble was adopted under the temperature of 298 K. Cutoff for van der Waals interactions and real space cutoff for electrostatic interactions are both set to 1.0 nm as reported.[32] The electrostatic interactions are calculated by using Particle-mesh Ewald method.[33] All simulations are performed with the Gromacs 4.5.5 package.[34] Every simulation runs for 6 ns with time step of 2 fs and snapshots in the last 2 ns are collected for data analysis during which the real time contact angle remains stable. The Lennard-Jones (L-J) parameters could be obtained from the adsorption energy according to the formula: $\varepsilon_{CO} = -0.0619\Delta E$.[25,35] In this case, by using the calculated results of adsorption energy of water molecule on graphene surface reported previously,[25] which was 98 meV, the L-J parameters for carbon atom are calculated to be $\varepsilon_C = 0.5365$ kJ mol^{-1} and $\sigma_C = 0.3689$ nm, respectively, under the rule of $\varepsilon_{CO} = \sqrt{\varepsilon_C \cdot \varepsilon_O}$ and $\sigma_{CO} = (\sigma_C + \sigma_O)/2$.

The first-principles simulations for water molecules on graphene are carried out within the framework of density functional theory using the Vienna ab initio simulation package (VASP) code.[36] The Perdew-Burke-Ernzerhoff (PBE) functional with general gradient approximation (GGA) was employed, and the ion-electron interactions are described by using the projector-augmented wave (PAW) method.[37] The hybrid functional BLYP and B3LYP was also used to verify the results.[38] The van der Waals interactions D3 corrections are invoked in all the simulations.[39] The energy cutoff of the plane-wave basis was 700 eV. Both one-leg and two-leg configurations of water molecule are considered in this

work. The 5 × 5 graphene supercell contains a vacuum layer ≈15 Å and its structure was optimized until the force component on every atom was less than 0.01 eV $Å^{-1}$. The Brillouin zone was integrated using the k mesh of 3 × 3 × 1.

Supporting Information

Supporting Information is available from the Wiley Online Library or from the author.

Acknowledgements

J.C.Z., K.C.J., and Y.F.H. contributed equally to this work. This work was financially supported by the Beijing National Laboratory for Molecular Sciences (Grant No. BNLMS- CXTD-202001), National Basic Research Program of China (Grant Nos. 2016YFA0200101 and 2018YFA0703502), Beijing Municipal Science & Technology Commission (Grant Nos. Z181100004818001, Z18110300480002, Z191100000819005, Z191100000819007, and Z201100008720005), and National Natural Science Foundation of China (Grant Nos. 21525310, 52072042, and 11904389). The computational resources were supported by the Platform for Data-Driven Computational Materials Discovery at the Songshan Lake Materials Laboratory and the Center for Quantum Simulation Sciences in the Institute of Physics. The authors acknowledge the Electron Microscopy Laboratory of Peking University, China for the use of ESEM and TEM.

Conflict of Interest

The authors declare no conflict of interest.

Data Availability Statement

The data that support the findings of this study are available in the supplementary material of this article.

Keywords

clean graphene, environmental scanning electron microscopy, intrinsic wettability, water contact angle

Received: May 12, 2021
Revised: November 16, 2021
Published online: December 16, 2021

[1] a) S. Hu, M. Lozada-Hidalgo, F. C. Wang, A. Mishchenko, F. Schedin, R. R. Nair, E. W. Hill, D. W. Boukhvalov, M. I. Katsnelson, R. A. W. Dryfe, I. V. Grigorieva, H. A. Wu, A. K. Geim, *Nature* **2014**, *516*, 227; b) L. Chen, G. Shi, J. Shen, B. Peng, B. Zhang, Y. Wang, F. Bian, J. Wang, D. Li, Z. Qian, G. Xu, G. Liu, J. Zeng, L. Zhang, Y. Yang, G. Zhou, M. Wu, W. Jin, J. Li, H. Fang, *Nature* **2017**, *550*, 380; c) M. Lozada-Hidalgo, S. Hu, O. Marshall, A. Mishchenko, A. N. Grigorenko, R. A. W. Dryfe, B. Radha, I. V. Grigorieva, A. K. Geim, *Science* **2016**, *351*, 68.

[2] a) M. Ma, G. Tocci, A. Michaelides, G. Aeppli, *Nat. Mater.* **2016**, *15*, 66; b) D. V. Andreeva, M. Trushin, A. Nikitina, M. C. F. Costa, P. V. Cherepanov, M. Holwill, S. Y. Chen, K. Yang, S. W. Chee, U. Mirsaidov, A. C. H. Neto, K. S. Novoselov, *Nat. Nanotechnol.* **2021**, *16*, 174.

[3] J. Wang, W. Gao, H. Zhang, M. H. Zou, Y. Chen, Y. Zhao, *Sci. Adv.* **2018**, *4*, eaat7392.

[4] a) J. Yin, Z. H. Zhang, X. M. Li, J. X. Zhou, W. L. Guo, *Nano Lett.* **2012**, *12*, 1736; b) Y. W. Zhu, S. Murali, M. D. Stoller, K. J. Ganesh, W. W. Cai, P. J. Ferreira, A. Pirkle, R. M. Wallace, K. A. Cychosz, M. Thommes, D. Su, E. A. Stach, R. S. Ruoff, *Science* **2011**, *332*, 1537.

[5] P. Snapp, J. M. Kim, C. Cho, J. Leem, M. F. Haque, S. Nam, *npg Asia Mater.* **2020**, *12*, 22.

[6] a) J. Feng, Z. Guo, *Nanoscale Horiz.* **2019**, *4*, 339; b) J. Liu, C.-Y. Lai, Y.-Y. Zhang, M. Chiesa, S. T. Pantelides, *RSC Adv.* **2018**, *8*, 16918.

[7] D. Parobek, H. Liu, *2D Mater.* **2015**, *2*, 032001.

[8] Z. T. Li, Y. J. Wang, A. Kozbial, G. Shenoy, F. Zhou, R. McGinley, P. Ireland, B. Morganstein, A. Kunkel, S. P. Surwade, L. Li, H. T. Liu, *Nat. Mater.* **2013**, *12*, 925.

[9] A. I. Aria, P. R. Kidambi, R. S. Weatherup, L. Xiao, J. A. Williams, S. Hofmann, *J. Phys. Chem. C* **2016**, *120*, 2215.

[10] L. A. Belyaeva, P. M. G. van Deursen, K. I. Barbetsea, G. F. Schneider, *Adv. Mater.* **2018**, *30*, 1703274.

[11] J. Rafiee, X. Mi, H. Gullapalli, A. V. Thomas, F. Yavari, Y. Shi, P. M. Ajayan, N. A. Koratkar, *Nat. Mater.* **2012**, *11*, 217.

[12] J. E. Andrews, Y. Wang, S. Sinha, P. W. Chung, S. Das, *J. Phys. Chem. C* **2017**, *121*, 10010.

[13] R. Raj, S. C. Maroo, E. N. Wang, *Nano Lett.* **2013**, *13*, 1509.

[14] A. V. Prydatko, L. A. Belyaeva, L. Jiang, L. M. C. Lima, G. F. Schneider, *Nat. Commun.* **2018**, *9*, 4185.

[15] A. Ashraf, Y. B. Wu, M. C. Wang, K. Yong, T. Sun, Y. H. Jing, R. T. Haasch, N. R. Aluru, S. Nam, *Nano Lett.* **2016**, *16*, 5318.

[16] L. Lin, B. Deng, J. Sun, H. Peng, Z. Liu, *Chem. Rev.* **2018**, *118*, 9281.

[17] L. Lin, H. L. Peng, Z. F. Liu, *Nat. Mater.* **2019**, *18*, 520.

[18] L. Lin, J. C. Zhang, H. S. Su, J. Y. Li, L. Z. Sun, Z. H. Wang, F. Xu, C. Liu, S. Lopatin, Y. H. Zhu, K. C. Jia, S. L. Chen, D. R. Rui, J. Y. Sun, R. W. Xue, P. Gao, N. Kang, Y. Han, H. Q. Xu, Y. Cao, K. S. Novoselov, Z. Q. Tian, B. Ren, H. L. Peng, Z. F. Liu, *Nat. Commun.* **2019**, *10*, 1972.

[19] J. Zhang, L. Lin, L. Sun, Y. Huang, A. L. Koh, W. Dang, J. Yin, M. Wang, C. Tan, T. Li, Z. Tan, Z. Liu, H. Peng, *Adv. Mater.* **2017**, *29*, 1700639.

[20] A. C. Ferrari, D. M. Basko, *Nat. Nanotechnol.* **2013**, *8*, 235.

[21] L. G. Cançado, A. Jorio, E. H. M. Ferreira, F. Stavale, C. A. Achete, R. B. Capaz, M. V. O. Moutinho, A. Lombardo, T. S. Kulmala, A. C. Ferrari, *Nano Lett.* **2011**, *11*, 3190.

[22] J. E. Lee, G. Ahn, J. Shim, Y. S. Lee, S. Ryu, *Nat. Commun.* **2012**, *3*, 1024.

[23] N. A. Stelmashenko, J. P. Craven, A. M. Donald, E. M. Terentjev, B. L. Thiel, *J. Microsc.* **2001**, *204*, 172.

[24] J. Ma, A. Michaelides, D. Alfè, L. Schimka, G. Kresse, E. Wang, *Phys. Rev. B* **2011**, *84*, 033402.

[25] J. Zhang, K. Jia, L. Lin, W. Zhao, H. T. Quang, L. Sun, T. Li, Z. Li, X. Liu, L. Zheng, R. Xue, J. Gao, Z. Luo, M. H. Rummeli, Q. Yuan, H. Peng, Z. Liu, *Angew. Chem., Int. Ed. Engl.* **2019**, *58*, 14446.

[26] Y. F. Huang, S. Meng, *J. Chem. Phys.* **2018**, *149*, 014706.

[27] S. B. A. Cassie, *Trans. Faraday Soc.* **1944**, *40*, 546.

[28] Z. Li, A. Kozbial, N. Nioradze, D. Parobek, G. J. Shenoy, M. Salim, S. Amemiya, L. Li, H. Liu, *ACS Nano* **2016**, *10*, 349.

[29] L. Wang, I. Meric, P. Y. Huang, Q. Gao, Y. Gao, H. Tran, T. Taniguchi, K. Watanabe, L. M. Campos, D. A. Muller, J. Guo, P. Kim, J. Hone, K. L. Shepard, C. R. Dean, *Science* **2013**, *342*, 614.

[30] A. V. Kretinin, Y. Cao, J. S. Tu, G. L. Yu, R. Jalil, K. S. Novoselov, S. J. Haigh, A. Gholinia, A. Mishchenko, M. Lozada, T. Georgiou, C. R. Woods, F. Withers, P. Blake, G. Eda, A. Wirsig, C. Hucho, K. Watanabe, T. Taniguchi, A. K. Geim, R. V. Gorbachev, *Nano Lett.* **2014**, *14*, 3270.

[31] H. J. Berendsen, J. P. Postma, W. F. van Gunsteren, J. Hermans, *Intermolecular Forces*, Springer, Dordrecht, Netherlands **1981**, p. 331.
[32] C. Wang, H. Lu, Z. Wang, P. Xiu, B. Zhou, G. Zuo, R. Wan, J. Hu, H. Fang, *Phys. Rev. Lett.* **2009**, *103*, 137801.
[33] T. Darden, D. York, L. Pedersen, *J. Chem. Phys.* **1993**, *98*, 10089.
[34] B. Hess, C. Kutzner, D. Van Der Spoel, E. Lindahl, *J. Chem. Theory Comput.* **2008**, *4*, 435, 2008.
[35] T. Werder, J. H. Walther, R. Jaffe, T. Halicioglu, P. Koumoutsakos, *J. Phys. Chem. B* **2003**, *107*, 1345.
[36] G. Kresse, J. Hafner, *Phys. Rev. B* **1993**, *47*, 558.
[37] P. E. Blochl, *Phys. Rev. B* **1994**, *50*, 17953.
[38] a) A. D. Becke, *Phys. Rev. A* **1988**, *38*, 3098; b) C. Lee, W. Yang, R. G. Parr, *Phys. Rev. B* **1988**, *37*, 785.
[39] S. Grimme, S. Ehrlich, L. Goerigk, *J. Comput. Chem.* **2011**, *32*, 1456.